Journal of
Clinical Medicine

MDPI

Article

Impact of Diffusion Magnetic Resonance Imaging Preprocessing Steps on the DTI-ALPS Index

Chang-Soo Yun [1], Sewon Lim [2], Jun-Young Chung [3,*], Youngjin Lee [4,*] and for the Alzheimer's Disease Neuroimaging Initiative [†]

[1] Neuroscience Research Institute, Gachon University Gil Medical Center, 24, Namdong-daero 774beon-gil, Namdong-gu, Incheon 21565, Republic of Korea
[2] Department of Health Science, General Graduate School of Gachon University, 191, Hambangmoe-ro, Yeonsu-gu, Incheon 21936, Republic of Korea
[3] Department of Neuroscience, College of Medicine, Gachon University, 38-13, Dokjeom-ro 3beon-gil, Namdong-gu, Incheon 21565, Republic of Korea
[4] Department of Radiological Science, Gachon University, 191, Hambangmoe-ro, Yeonsu-gu, Incheon 21936, Republic of Korea
* Correspondence: jychung@gachon.ac.kr (J.-Y.C.); yj20@gachon.ac.kr (Y.L.); Tel.: +82-32-822-8251 (J.-Y.C.); +82-32-820-4362 (Y.L.)
† Details on the collaborators of the group Name are provided in the Acknowledgment. Data used in preparation of this article were obtained from the Alzheimer's Disease Neuroimaging Initiative (ADNI) database (adni.loni.usc.edu). As such, the investigators within the ADNI contributed to the design and implementation of ADNI and/or provided data but did not participate in analysis or writing of this report. A complete listing of ADNI investigators can be found at: http://adni.loni.usc.edu/wp-content/uploads/how_to_apply/ADNI_Acknowledgement_List.pdf.

Abstract

Background/Objectives: The diffusion tensor image analysis along the perivascular space (DTI-ALPS) index is a non-invasive glymphatic function marker. Derived from the ratio of orthogonal diffusivities, it may be susceptible to systematic bias from diffusion magnetic resonance imaging (dMRI) preprocessing. This study quantitatively evaluated the effect of individual preprocessing steps on the DTI-ALPS index. **Methods**: The dMRI and T1-weighted images of 100 cognitively normal participants under an identical protocol were obtained from the Alzheimer's Disease Neuroimaging Initiative. Six conditions were derived from identical source data: no preprocessing; four single-step pipelines (denoising, Gibbs ringing correction, eddy current/motion correction, or bias field correction); and full preprocessing. **Results**: Significant differences in the DTI-ALPS index were observed across preprocessing conditions ($\chi^2(5) = 97.947$, $p < 0.001$), with a modest overall effect size (Kendall's W = 0.196). Relative to the no-preprocessing condition, Gibbs ringing correction decreased the index by 0.63% on average (SD of percentage change, 0.72%), while eddy current and motion correction decreased it by 0.31% on average but showed greater interindividual variability (SD, 2.36%). The full preprocessing pipeline resulted in a mean decrease of 0.54%. Denoising and bias field correction produced no significant changes. Thus, despite statistical significance for several preprocessing conditions, the magnitude of the observed changes in the DTI-ALPS index was small. **Conclusions**: Individual preprocessing steps differentially affect the DTI-ALPS index. Gibbs ringing correction contributed the most consistent effect, while eddy current and motion correction exerted a significant, independent effect. These findings indicate that specific preprocessing steps can introduce statistically detectable but quantitatively small changes in the DTI-ALPS index. Standardized preprocessing may therefore be particularly important for cross-study harmonization, meta-analyses, and longitudinal or serial monitoring, where subtle differences in the DTI-ALPS index may affect comparability.

Check for updates

Academic Editor: Martin R. Prince

Received: 27 August 2026
Revised: 13 October 2026
Accepted: 12 November 2026
Published: 16 November 2026

Copyright: © 2026 by the authors. Licensee MDPI, Basel, Switzerland. This article is an open access article distributed under the terms and conditions of the Creative Commons Attribution (CC BY) license.

Keywords: glymphatic system; diffusion magnetic resonance imaging preprocessing; Alzheimer's disease; DTI-ALPS index

1. Introduction

The glymphatic system is a physiological mechanism for clearing waste products that accumulate in the brain. Cerebrospinal fluid (CSF) moves along the periarterial space and enters the brain parenchyma through aquaporin-4 water channels expressed on astrocyte endfeet, exchanges with interstitial fluid, and is subsequently drained via the perivenous space [1–3]. In addition to being essential for maintaining brain homeostasis, the glymphatic system has been reported to clear neurotoxic proteins such as amyloid beta and tau and has drawn attention as a key mechanism underlying the pathophysiology of neurodegenerative disorders [4,5].

As the physiological function and importance of the glymphatic system have come to the fore, various magnetic resonance imaging (MRI) techniques have been used to evaluate glymphatic function in the brain. Early studies employed contrast-enhanced MRI, in which a gadolinium-based contrast agent was administered intrathecally, and the resulting signal changes were tracked over several hours [6–9]. This approach enabled direct observation of the influx and clearance of CSF and served as a reference for subsequent methods. However, this approach requires an invasive procedure and repeated imaging for more than 24 h, and adverse effects associated with the use of contrast agents may occur, limiting its applicability to large-scale studies and routine clinical practice [10]. Thus, the demand for non-invasive methods that can assess the glymphatic system without contrast agents or invasive procedures has grown. To address these limitations of contrast-enhanced approaches, namely their invasiveness and the extended acquisition they require, diffusion MRI (dMRI), which quantifies the motion of water molecules in the brain, has been widely adopted for evaluating glymphatic function [11–15].

Diffusion MRI is widely used in clinical and research protocols, offering the practical advantage that retrospective analyses can be performed without additional acquisition. For this reason, a variety of approaches have been proposed, including attempts to isolate the diffusion component of CSF using multiple *b*-value schemes that incorporate low *b*-values, approaches that examine the glymphatic system using diffusion kurtosis imaging, and approaches that utilize directional diffusivities derived from diffusion tensor imaging (DTI) [13–15]. Among the various attempts using dMRI, Taoka et al. proposed in 2017 the diffusion tensor image analysis along the perivascular space (DTI-ALPS) index, which evaluates the perivascular space using DTI [11]. This method exploits the anatomical feature that, at the level of the lateral ventricle body, the deep medullary veins run in the left-right (e.g., *x*-axis) direction, whereas the projection fibers (e.g., *z*-axis) and association fibers (e.g., *y*-axis) at the same location run perpendicular to them. The *x*-axis is perpendicular to the orientation of both fiber tracts. Diffusivity measured along this axis is assumed to reflect movement within the perivascular space. The DTI-ALPS index is calculated as the ratio of the *x*-axis diffusivity in the projection and association fiber regions to the diffusivity along their respective perpendicular directions. The DTI-ALPS index has been widely used as an indirect measure of glymphatic function in a range of disease groups [15–19].

The DTI-ALPS index is derived from the ratio of tensor components estimated from dMRI signals and is inherently contingent upon the fidelity of diffusion tensor estimation. Previous studies have demonstrated that the DTI-ALPS index varies according to acquisition parameters, including the *b*-value, the number of diffusion gradient directions, and the spatial resolution, as well as the degree of head rotation and the criteria adopted for region-

of-interest (ROI) placement [20–23]. The dMRI preprocessing procedures applied after image acquisition also determine the stability of the DTI-ALPS index. dMRI is susceptible to a range of artifacts, including thermal noise, Gibbs ringing, eddy current-induced geometric distortion, subject head motion, and signal bias attributable to receiver coil sensitivity inhomogeneity [24]. To mitigate these effects, standard dMRI preprocessing pipelines routinely incorporate denoising, Gibbs ringing correction, eddy current and motion correction, and bias field correction. The effects of these dMRI preprocessing procedures on diffusion tensor estimation and conventional diffusion metrics such as fractional anisotropy (FA) and mean diffusivity have been relatively well characterized [25]. However, the influence of each preprocessing step on the DTI-ALPS index remains unclear, and the reproducibility of the reported values has not been systematically evaluated. This question is of particular importance because the DTI-ALPS index is calculated as the ratio of the diffusivities measured along mutually orthogonal directions. Artifacts that affect diffusion measurements unequally across directions may therefore introduce systematic bias into the DTI-ALPS index unless adequately corrected. Such bias would limit the comparability of the DTI-ALPS index across studies employing different preprocessing pipelines and would compromise the reliability of the DTI-ALPS index as a biomarker of glymphatic function.

This study aimed to quantitatively evaluate the influence of dMRI preprocessing on the DTI-ALPS index. A single-step approach was employed in which raw data without any preprocessing were compared with four conditions, each constructed by applying only a single preprocessing step —denoising, Gibbs ringing correction, eddy current and motion correction, or bias field correction—and with a full preprocessing condition. The DTI-ALPS index computed under each condition was subsequently compared within a cohort of cognitively normal individuals, enabling assessment of the effect of each preprocessing step on the absolute magnitude and variability of the DTI-ALPS index. The findings are intended to establish an empirical basis for the preprocessing requirements governing the computation of the DTI-ALPS index and contribute to methodological standardization in subsequent investigations.

2. Materials and Methods

2.1. Participants

The data used in this study were obtained from the Alzheimer's Disease Neuroimaging Initiative (ADNI) database (adni.loni.usc.edu), encompassing the ADNI-1, ADNI-2, and ADNI-3 phases. Given that variability in scanner hardware and acquisition parameters constitutes a well-recognized source of heterogeneity in diffusion metrics, and that such variability would confound the isolated assessment of preprocessing effects, the analysis was restricted to participants scanned on the same scanner model under an identical acquisition protocol. Participants were included if diffusion-weighted images and corresponding T1-weighted images acquired at the same visit were available and if they were classified as cognitively normal (CN) at that visit. ADNI diagnostic classification is based on standardized clinical and neuropsychological assessments, including the clinical dementia rating (CDR) and mini-mental state examination (MMSE). Participants classified as CN generally had a global CDR score of 0, an MMSE score within the normal range, and no evidence of significant cognitive impairment according to ADNI criteria. Participants with a non-CN diagnosis were excluded from the present analysis. Individuals were excluded if the imaging data exhibited severe artifacts, precluding reliable tensor estimation. The final analysis included 100 CN participants. Figure 1 presents a flow diagram detailing the participant selection process, including the number of individuals excluded at each stage.

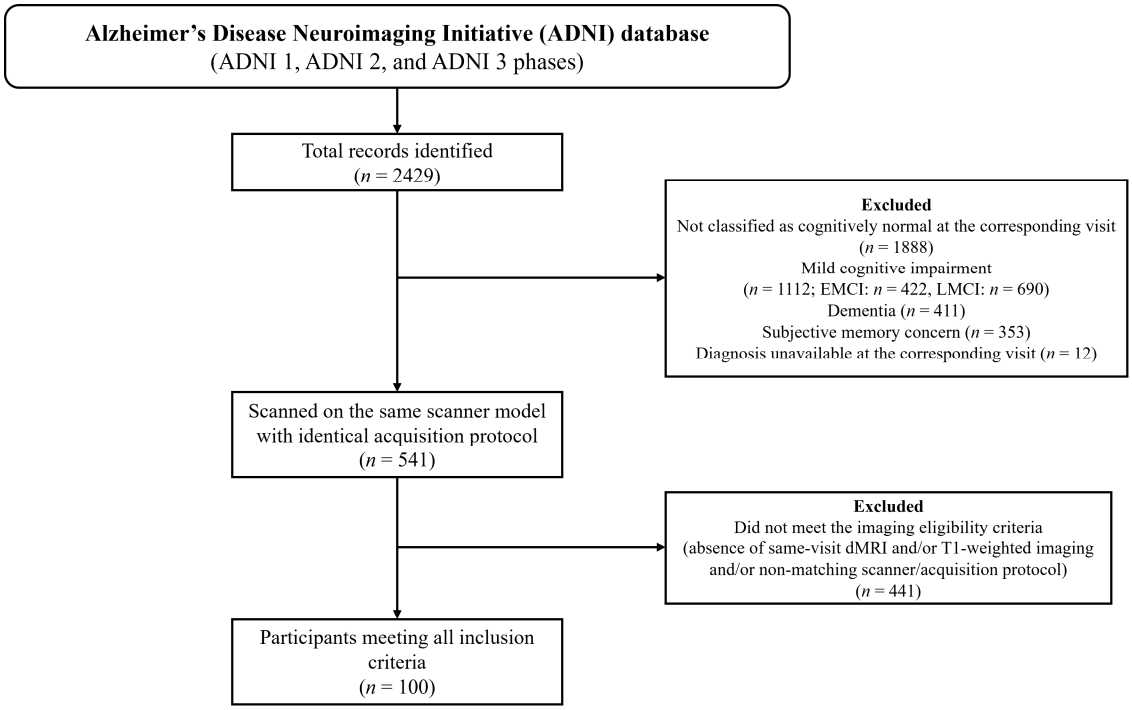


Figure 1. Flow diagram of the participant selection process, showing the number of records identified in the ADNI database, the number excluded at each stage, and the composition of the final sample.

2.2. Image Acquisition and Preprocessing

Diffusion-weighted images were acquired on a SIEMENS MAGNETOM Prisma 3T (Siemens Healthcare, Erlangen, Germany) using a single-shot echo-planar imaging sequence with the following parameters: repetition time, 10,700 ms; echo time, 95 ms; acquisition matrix, 1044 × 1044 mm^2; slice thickness, 2 mm; 31 diffusion gradient directions at b = 1000 s/mm^2; and five nondiffusion-weighted (b = 0 s/mm^2) volumes.

MRI data included in the present study were acquired between 2017 and 2023 as part of the ADNI-1, ADNI-2, and ADNI-3. All dMRI preprocessing was implemented using MRtrix3 (version 3.0.3) and FSL (version 6.0.1). The complete pipeline comprised four sequential correction steps: (1) denoising based on Marchenko–Pastur principal component analysis (MP-PCA), which suppresses thermal noise by identifying and removing noise-only principal components within a local sliding window (5 × 5 × 5 voxels) according to random matrix theory; this step was applied first to the raw data because MP-PCA assumes spatially uncorrelated noise, which is violated by interpolation in subsequent steps (dwidenoise); (2) Gibbs ringing correction using the method of local subvoxel shifts (mrdegibbs); (3) eddy current-induced distortion and head motion correction (eddy_cuda). For conditions including eddy correction, the rotated b-vectors generated by eddy_cuda were propagated to subsequent diffusion tensor fitting, whereas the original b-vectors were retained for conditions without eddy correction; and (4) B1 field inhomogeneity correction based on the N4 algorithm (dwibiascorrect ants). Six preprocessing conditions were constructed to isolate the contribution of each step. The Raw condition comprised unprocessed raw data to which none of the four preprocessing steps were applied. Four single-step conditions were generated by applying only one preprocessing procedure to the raw data and were designated Denoise_only, Degibbs_only, Eddy_only, and Bias_only. The Full condition comprised all four preprocessing procedures applied sequentially in the order described above. All conditions were derived from identical source data, such that any observed difference in the resulting index was attributable solely to the applied step in the single-step preprocessing conditions. In addition, the wall-clock execution time for

each preprocessing step was recorded for each participant under all the conditions. All processing was performed on a single workstation (CPU: Intel, Santa Clara, CA USA, Core Ultra 7 265 K @ 5.5 GHz; RAM: Samsung, South Korea, 16 GB × 4 DDR5; GPU: NVIDIA, Santa Clara, CA, USA, RTX 5070 12 GB), with participants processed sequentially so that the recorded times were comparable across conditions. The total processing time per participant was obtained by summing the times of all the steps constituting each condition.

For each of the six conditions, the diffusion tensor was fitted on a voxel-wise basis using weighted least squares (dtifit –wls), yielding the diffusion tensor elements and the FA map. To ensure that differences among conditions reflected preprocessing rather than spatial registration, a single transformation was estimated for each participant and shared across all conditions. The FA map of the Full condition was linearly registered to the FMRIB58_FA standard-space template using FLIRT, followed by nonlinear refinement using FNIRT, and the resulting warp field was inverted (invwarp). The standard-space projection and association fiber ROIs were then transformed into each participant's native diffusion space using this inverse warp with nearest-neighbor interpolation and restricted to the brain mask. The DTI-ALPS index was calculated from the native-space tensor elements (Dxx, Dyy, and Dzz) within these ROIs, which obviated the need for tensor reorientation. The overall diffusion MRI preprocessing workflow, including the full preprocessing pipeline and individual preprocessing conditions, is illustrated in Figure 2.

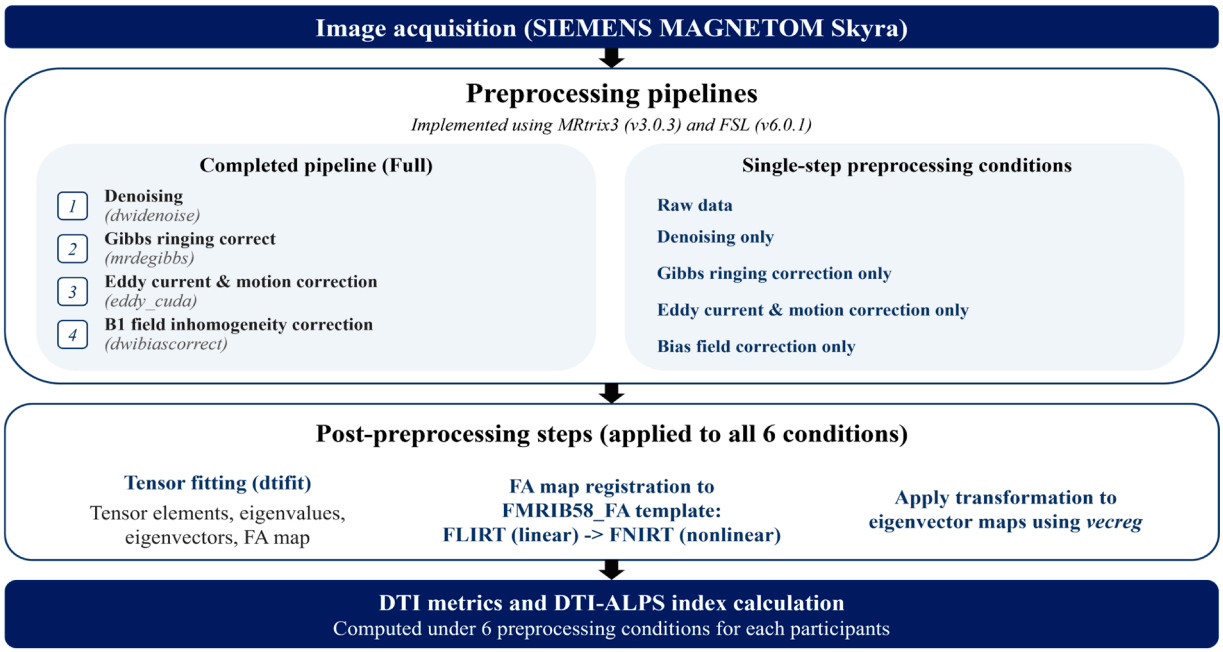


Figure 2. Schematic overview of the diffusion MRI acquisition and processing workflow. Six preprocessing conditions were evaluated: the Raw condition, in which no preprocessing was applied; four single-step conditions, in which denoising, Gibbs ringing correction, eddy current and motion correction, or bias field correction was applied individually; and the Full condition, in which all four preprocessing procedures were applied sequentially. Tensor estimation, spatial registration, and DTI-ALPS analysis were subsequently performed identically for all conditions.

2.3. Calculation of the DTI-ALPS Index

The DTI-ALPS index was calculated using the method described by Taoka et al. [11]. Spherical ROIs with a 5-mm diameter were placed at the level of the lateral ventricle body, where the deep medullary veins course predominantly along the *x*-axis [11]. ROIs were positioned in the projection and association fiber areas of the left hemisphere, yielding

two regions, which were identified as regions exhibiting predominantly z-axis and y-axis orientations, respectively, on the color-coded FA map of the template. ROIs were defined once in the FMRIB58 standard space using fixed coordinates and applied uniformly across all participants and preprocessing conditions. This procedure eliminated inter- and intra-rater variability in ROI placement, thereby minimizing ROI placement-related variability across preprocessing conditions.

Within each region, the diffusivity along each principal axis was extracted, and the DTI-ALPS index was calculated as follows:

$$DTI-ALPS\ index = \frac{mean\left(Dxx_{proj},\ Dxx_{asso}\right)}{mean\left(Dyy_{proj},\ Dzz_{asso}\right)} \quad (1)$$

where Dxx_{proj} and Dxx_{asso} represent the diffusivity along the x-axis within the projection and association fiber areas, respectively, and Dyy_{proj} and Dzz_{asso} represent the diffusivity along the directions perpendicular to the corresponding fiber orientations, namely the y-axis in the projection fiber area and the z-axis in the association fiber area. In standard space, the ROIs were placed at (x, y, z) = (−26, −17, 29) for the projection fiber area and (x, y, z) = (−37, −17, 29) for the association fiber area, with the coordinates adopted from those reported in previous studies [11]. Because these coordinates were applied identically to every participant and to all preprocessing conditions, the ROI placement itself introduced no variance into the comparisons. Figure 3 illustrates the locations of the predefined projection and association fiber ROIs in standard space.

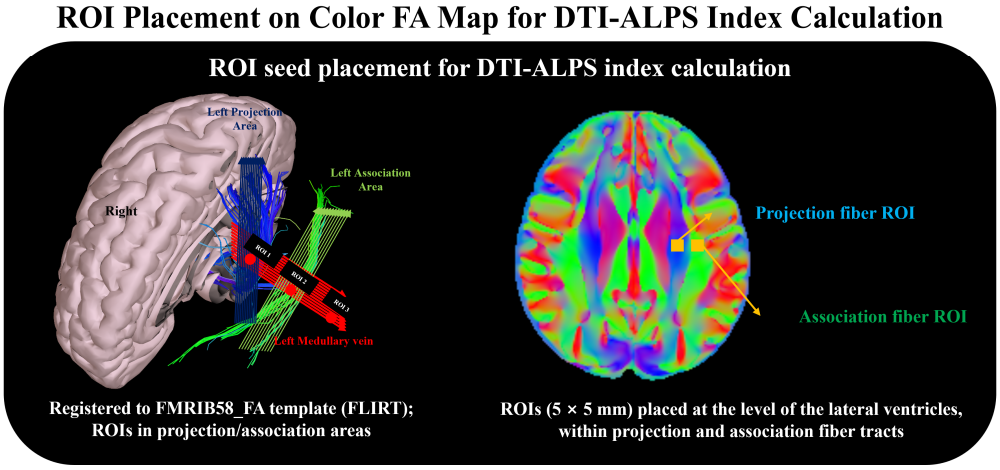


Figure 3. Region of interest (ROI) placement on the color-coded FA map for computation of the DTI-ALPS index. (**Left**), schematic showing the deep medullary vein and the perpendicular orientation of the projection (blue) and association (green) fiber areas used to define the ROIs, registered to the FMRIB58_FA standard-space template. (**Right**), representative color-coded FA map showing the projection and association fiber ROIs placed at the level of the lateral ventricle body.

2.4. Statistical Analysis

The normality of the DTI-ALPS index distribution was assessed using the Shapiro–Wilk test [26]. Given the repeated-measures structure of the single-step design, nonparametric procedures were adopted. The six conditions were compared within the CN group using the Friedman test [27], which accounted for the repeated-measures structure arising from the application of all conditions to the same participants. Where the Friedman test yielded a significant result, post hoc pairwise comparisons based on mean rank differences were performed with Bonferroni adjustment for multiple comparisons.

Kendall's W was calculated to quantify the overall effect size of the Friedman test. Additionally, paired mean differences and standardized effect sizes (Cohen's dz) were

calculated for each preprocessing condition relative to the no-preprocessing condition. A retrospective sensitivity analysis was performed using a paired t-test approximation to estimate the minimum detectable effect (MDE), assuming 80% statistical power and a two-sided nominal significance level of 0.05. The MDE estimates were considered supplementary measures of statistical sensitivity rather than the exact detectable effects of the rank-based multiple comparison procedure. Statistical analysis was conducted using MATLAB (R2026a, Natick, MA, USA: The MathWorks Inc.), and a p-value < 0.05 was considered statistically significant.

3. Results

3.1. Effects of Preprocessing Conditions on the DTI-ALPS Index

Descriptive statistics for the DTI-ALPS index under the six preprocessing conditions are presented in Table 1. In the CN group, the Friedman test revealed a significant difference among the six conditions ($\chi^2(5) = 97.947$, $p < 0.001$, Kendall's W = 0.196). Bonferroni-adjusted post hoc pairwise comparisons using the no-preprocessing condition as the reference showed significant differences for the Degibbs_only (adjusted $p < 0.001$), Eddy_only (adjusted $p = 0.046$), and the Full conditions (adjusted $p < 0.001$). In contrast, neither the Denoise_only condition (adjusted $p = 0.493$) nor the Bias_only condition (adjusted $p = 1.000$) differed significantly from the no-preprocessing condition.

A retrospective sensitivity analysis indicated a minimum detectable standardized effect size of approximately Cohen's dz = 0.28, assuming 80% statistical power and a two-sided nominal significance level of 0.05. Denoising produced a mean change of +0.0049 (dz = 0.282), approximately corresponding to the estimated MDE of 0.0049. Gibbs ringing correction showed a larger standardized effect (mean change = −0.0093, dz = −0.730), exceeding its estimated MDE of 0.0036. In contrast, eddy current and motion correction produced a smaller standardized effect (mean change = −0.0044, dz = −0.119), below its estimated MDE of 0.0105. Similarly, Full preprocessing produced a mean change of −0.0079 (dz = −0.236), below its estimated MDE of 0.0095. For bias field correction, the recorded DTI-ALPS index values were identical to those obtained without preprocessing in all 100 participants. These MDE estimates were based on a paired t-test approximation and do not directly represent the statistical sensitivity of the Bonferroni-adjusted rank-based comparisons.

Table 1. Descriptive statistics for the DTI-ALPS index under the six preprocessing conditions in the CN group ($n = 100$). Mean ranks were derived from the Friedman test. SD, standard deviation.

Condition	Mean ± SD	Median	Q1–Q3	Mean Rank	Adjusted p
None	1.402 ± 0.167	1.401	1.296–1.523	4.015	—
Denoising only	1.407 ± 0.170	1.408	1.298–1.521	4.475	0.493
Gibbs ringing correction only	1.392 ± 0.162	1.394	1.286–1.513	2.360	<0.001
Eddy current only	1.397 ± 0.172	1.394	1.272–1.518	3.310	0.046
Bias field correction only	1.402 ± 0.167	1.401	1.296–1.523	4.015	1.000
Full preprocessing	1.394 ± 0.168	1.391	1.284–1.513	2.825	<0.001

Relative to the no-preprocessing condition, application of Gibbs ringing correction produced the largest mean change in the DTI-ALPS index, decreasing it by 0.63% on average (mean difference, −0.0093). This decrease was highly consistent across participants, with 88 of the 100 participants exhibiting a lower value, 10 exhibiting a higher value, and two showing no numerical change. Eddy current and motion correction produced a smaller mean decrease of 0.31% (mean difference, −0.0044), with 59 participants showing a decrease, 38 showing an increase, and three showing no numerical change. In contrast,

denoising resulted in a modest mean increase of 0.34% (mean difference, +0.0049), with 60 participants showing an increase, 34 showing a decrease, and six showing no numerical change. Bias field correction produced no numerical changes in the DTI-ALPS index in any of the 100 participants. The Full condition resulted in a mean decrease of 0.54% relative to the no-preprocessing condition (mean difference, −0.0079), with 64 participants showing a decrease, 34 showing an increase, and two showing no numerical change. The changes in the DTI-ALPS index across preprocessing conditions, including mean and median differences, percentage changes, and the number of participants showing increased, decreased, or unchanged values, are summarized in Table 2.

Table 2. Direction and magnitude of changes in the DTI-ALPS index relative to the no-preprocessing condition in the CN group ($n = 100$). Mean and median differences were calculated as each preprocessing condition minus the no-preprocessing condition. Mean change (%) represents the mean of participant-level percentage changes relative to the no-preprocessing condition.

Condition	Mean Difference	Median Difference	Mean Change (%)	Increased	Decreased	Unchanged
Denoising only	0.0049	0.0025	0.34	60	34	6
Gibbs ringing correction only	−0.0093	−0.0090	−0.63	10	88	2
Eddy current only	−0.0044	−0.0065	−0.31	38	59	3
Bias field correction only	0	0	0	0	0	100
Full preprocessing	−0.0079	−0.0090	−0.54	34	64	2

3.2. Processing Time Across Preprocessing Conditions

The total processing time per participant differed markedly across the six preprocessing conditions. The mean processing time under the no-preprocessing condition was 12.22 ± 2.43 s. Application of denoising, Gibbs ringing correction, and bias field correction increased the processing time to 18.48 ± 4.60 s, 16.89 ± 4.46 s, and 15.61 ± 2.63 s, corresponding to increases of 51.22%, 38.26%, and 27.77%, respectively. Eddy current and motion correction required substantially more processing time, with a mean of 178.98 ± 18.39 s, representing a 1364.88% increase relative to the no-preprocessing condition. The Full preprocessing condition required the longest processing time, with a mean of 231.73 ± 17.72 s, corresponding to a 1796.32% increase relative to the no-preprocessing condition. The processing times for all six conditions are summarized in Table 3.

Table 3. Processing time per participant under the six preprocessing conditions. Values are presented as mean ± standard deviation across 100 cognitively normal participants. The percentage increase in processing time was calculated relative to the no-preprocessing condition.

Condition	Processing Time (s), Mean ± SD	Increase vs. None (%)
None	12.22 ± 2.43	—
Denoising only	18.48 ± 4.60	51.22
Gibbs ringing correction only	16.89 ± 4.46	38.26
Eddy current correction only	178.98 ± 18.39	1364.88
Bias field correction only	15.61 ± 2.63	27.77
Full preprocessing	231.73 ± 17.72	1796.32

4. Discussion

This study evaluated the influence of individual dMRI preprocessing procedures on the DTI-ALPS index using a single-step preprocessing design. The magnitude and direction of the effects varied substantially across the preprocessing procedures. Relative to the no-preprocessing condition, significant changes in the DTI-ALPS index were observed following Gibbs ringing correction, eddy current and motion correction, and application of the full

preprocessing pipeline, whereas denoising and bias field correction were not associated with significant alterations. Furthermore, marked differences were observed in the consistency of these effects among participants, indicating that individual preprocessing procedures influenced the DTI-ALPS index through distinct mechanisms rather than through a uniform modification of diffusion measurements.

Application of Gibbs ringing correction produced the largest mean change among the individual preprocessing procedures, resulting in an average decrease of 0.63% in the DTI-ALPS index (mean difference, −0.0093). The direction of this effect was highly consistent across participants, with lower values observed in 88 of the 100 individuals following correction. This pronounced directional consistency suggests a systematic rather than predominantly random influence of Gibbs ringing on the DTI-ALPS index. The ROIs used for DTI-ALPS analysis were located at the level of the lateral ventricular body within a few voxels of the boundary between the ventricular CSF and adjacent white matter, where the sharp tissue-intensity transition renders the region particularly susceptible to truncation-induced Gibbs ringing [28–30]. Gibbs ringing arises from finite k-space truncation and produces spatially oscillatory signal perturbations around sharp boundaries; its manifestation is dependent on the sampling direction and local image structure [28,31]. In dMRI, such perturbations may propagate differently across diffusion-weighted measurements and consequently introduce a direction-dependent bias into the estimated diffusion metrics. Because the ROIs were defined at fixed standard-space coordinates and sampled at broadly comparable locations relative to the ventricular boundary across the participants, a directional perturbation of this type could result in a consistent alteration in the DTI-ALPS index when the diffusivities contributing to the numerator and denominator are affected unequally. Therefore, our findings suggest that uncorrected Gibbs ringing systematically increases the DTI-ALPS index in this anatomical region.

A distinct pattern was observed following eddy current and motion correction. Application of this correction resulted in an average decrease of 0.31% in the DTI-ALPS index (mean difference, −0.0044), and a significant difference from the no-preprocessing condition was identified. However, the direction of individual changes was considerably more heterogeneous than that observed for the Gibbs ringing correction, with decreases in 59 participants, increases in 38 participants, and no numerical change in three participants. This distribution suggests a higher degree of participant-specific influence. Eddy current-induced distortion and head motion vary according to individual motion characteristics and image distortion patterns, and their effects on diffusion tensor estimation are therefore inherently heterogeneous across participants [32–34]. Accordingly, a relatively small mean change should be interpreted in conjunction with substantial inter-individual variability. Eddy current and motion correction may exert only modest effects in many participants while producing considerably larger alterations in a subset, emphasizing the importance of evaluating both the central tendency and distribution of individual changes when assessing their influence on the DTI-ALPS index.

Bias field correction had no measurable influence on the DTI-ALPS index. For the numerical precision used in the present analysis, identical values were obtained before and after bias field correction for all 100 CN participants. This finding is consistent with the mathematical characteristics of diffusion tensor estimation. Receiver coil sensitivity inhomogeneity represents a spatially smooth multiplicative modulation of signal intensity, whereas diffusivity is estimated from the logarithmic relationship between diffusion-weighted and non-diffusion-weighted signals [22,35–38]. Therefore, the multiplicative factor affecting both measurements to a comparable extent is largely canceled during tensor estimation. Under the acquisition and analytical conditions employed in the present study, B1 field inhomogeneity correction appeared to exert a negligible direct influence on the DTI-ALPS index.

Similarly, denoising was not associated with a statistically significant difference relative to the no-preprocessing condition, although its pattern of influence differed from that of bias field correction. An average increase of 0.34% in the DTI-ALPS index was observed following denoising (mean difference, +0.0049), with an increase in 60 participants, a decrease in 34 participants, and no numerical change in six participants. Thermal noise can affect diffusion tensor estimation through two principal mechanisms. First, random noise in the diffusion-weighted signals introduces stochastic errors into the fitted tensor elements, increasing the variance of the estimated diffusivities. Second, the noise in magnitude-reconstructed diffusion-weighted images can elevate low-intensity signals, potentially leading to systematic underestimation of diffusivity, particularly in directions with signal attenuation [39–43]. The relatively small and heterogeneous alterations observed in the present study suggest that a substantial proportion of this effect may be attenuated by the ratio-based formulation of the DTI-ALPS index. Spatial averaging within spherical ROIs may provide an additional reduction in the contribution of random voxel-level variability to the estimated directional diffusivities.

The Full preprocessing condition was associated with an average decrease of 0.54% in the DTI-ALPS index relative to the no-preprocessing condition (mean difference, −0.0079), and a statistically significant difference was observed between the two conditions. Notably, the magnitude of the net change produced by the full pipeline was smaller than that observed following the application of Gibbs ringing correction alone. This finding indicates that the effects of the individual preprocessing procedures cannot necessarily be regarded as independent contributions that combine linearly to determine the final DTI-ALPS index. Each procedure modifies the data supplied to subsequent processing stages, allowing interactions among preprocessing operations to attenuate, amplify, or otherwise modify the effects observed when individual procedures are applied in isolation. Therefore, the single-step design employed in this study provides information regarding the isolated direction and magnitude of influence attributable to each procedure, whereas the Full condition reflects the cumulative influence within a conventional sequential preprocessing framework.

The computational requirements also varied markedly among the preprocessing procedures. The no-preprocessing condition required 12.22 ± 2.43 s per participant. Application of denoising, Gibbs ringing correction, and bias field correction increased the mean processing time to 18.48 ± 4.60 s, 16.89 ± 4.46 s, and 15.61 ± 2.63 s, corresponding to increases of 51.22%, 38.26%, and 27.77%, respectively, relative to the no-preprocessing condition. Although these proportional increases appear substantial because of the short baseline processing time, the corresponding absolute computational burden was limited to approximately 3–6 additional seconds per participant. In contrast, eddy current and motion correction required 178.98 ± 18.39 s per participant, representing a 1364.88% increase relative to the no-preprocessing condition. The full preprocessing pipeline required the longest processing time, at 231.73 ± 17.72 s per participant, corresponding to an increase of 1796.32%. Therefore, eddy current and motion correction constituted the principal computational burden among the individual preprocessing procedures. Nevertheless, this procedure was associated with a significant change in the DTI-ALPS index. Gibbs ringing correction is particularly noteworthy in this context because it produced the most consistent alteration in the index while requiring only approximately 4.7 additional seconds per participant. Consequently, excluding the Gibbs ringing correction provides little practical computational advantage. Although the denoising and bias field corrections were not associated with measurable changes in the DTI-ALPS index, the additional computational requirements were modest. Collectively, these findings favor retention of a complete preprocessing pipeline for methodological standardization. In large-scale cohorts, for which processing time represents a substantial constraint, optimization, GPU acceleration, or parallelization

of eddy current and motion correction would constitute a more appropriate strategy than exclusion of individual preprocessing procedures.

The present study had several limitations that warrant consideration. First, the analysis was restricted to participants examined using a single-scanner model and an identical acquisition protocol. Although this restriction minimized acquisition-related heterogeneity and facilitated isolation of preprocessing effects, generalizability to other scanner platforms, spatial resolutions, diffusion-weighting schemes, and acquisition parameters remained limited. Second, despite the statistically significant overall difference among the preprocessing conditions, the effect size was modest (Kendall's W = 0.196); accordingly, the biological and clinical relevance of the observed numerical differences requires cautious interpretation. Also, the retrospective minimum detectable effect (MDE) analysis indicated that the observed mean changes associated with eddy current and motion correction (0.0044) and Full preprocessing (0.0079) were smaller than their respective estimated MDE (0.0105 and 0.0095) at 80% statistical power. Although both conditions demonstrated statistically significant differences from the no-preprocessing condition, these findings should be interpreted cautiously given the relatively small observed effects. Third, the single-step design was specifically intended to isolate the influence of the individual preprocessing procedures. However, an individual correction applied directly to otherwise unprocessed data may not reproduce its behavior when embedded in a sequential preprocessing pipeline. Interactions among preprocessing procedures may, therefore, account for the discrepancy between the effect of the full pipeline and the isolated effects of individual corrections. Fourth, formal analyses of the individual directional diffusivity components contributing to the DTI-ALPS index were beyond the scope of this study. Such analyses may provide additional mechanistic insights into the particularly consistent influence observed following Gibbs ringing correction. Fifth, because the ROIs were defined at fixed standard-space coordinates, residual differences in spatial registration may have contributed to a portion of the observed variability. Finally, the absolute processing times reported in the present study were dependent on the computational hardware, software versions, and implementation employed and should therefore not be interpreted as universally applicable benchmarks. Nevertheless, the relative differences between preprocessing procedures provide a practical indication of their computational burden under otherwise identical processing conditions.

5. Conclusions

This study demonstrated that individual dMRI preprocessing procedures exert differential but quantitatively small effects on the DTI-ALPS index. Among the individual procedures evaluated, Gibbs ringing correction produced the most consistent change in the DTI-ALPS index (mean change: −0.63%), whereas eddy current and motion correction were associated with a smaller but more heterogeneous effect across participants (mean change: −0.31%). In contrast, denoising and bias field correction did not produce statistically significant changes in the DTI-ALPS index under the acquisition and analytical conditions examined. The full preprocessing pipeline also produced a statistically significant but small change relative to the no-preprocessing condition (mean change: −0.54%), indicating that DTI-ALPS measurements are influenced by the preprocessing strategy applied. Although these findings demonstrate statistically detectable differences, their clinical significance remains uncertain given the small magnitude of the observed changes. Nevertheless, these results provide an empirical basis for understanding the preprocessing dependence of the DTI-ALPS index and suggest that consistent preprocessing procedures may facilitate methodological harmonization and comparability across studies, particularly when evaluating subtle longitudinal changes. Further research is needed to determine whether these preprocessing-related differences have meaningful implications for clinical interpretation.

Author Contributions: Conceptualization, C.-S.Y. and Y.L.; methodology, C.-S.Y., J.-Y.C. and Y.L.; software, C.-S.Y. and S.L.; validation, C.-S.Y., S.L. and Y.L.; formal analysis, C.-S.Y.; investigation, C.-S.Y. and S.L.; data curation, S.L.; writing—original draft preparation, C.-S.Y.; writing—review and editing, J.-Y.C. and Y.L.; project administration, J.-Y.C. and Y.L.; and funding acquisition, J.-Y.C. The investigators within the Alzheimer's Disease Neuroimaging Initiative (ADNI) contributed to the design and implementation of the ADNI study and/or provided data used in this research but did not participate in the data analysis or writing of this manuscript. All authors have read and agreed to the published version of the manuscript.

Funding: This work was supported by National Research Foundation of Korea (NRF) grants funded by the Korean government (MSIT) (grant numbers NRF-2022R1A2C2010363 and RS-2025-02303425).

Institutional Review Board Statement: This study was approved by the Institutional Review Board of Gachon University (IRB No.1044396-202607-HR-207-01, 13 August 2026).

Informed Consent Statement: The Alzheimer's Disease Neuroimaging Initiative (ADNI) dataset used in our study was collected with written informed consent from all participants. Details regarding ADNI study procedures and consent can be found at: https://adni.loni.usc.edu/wp-content/themes/freshnews-dev-v2/documents/policy/ADNI_Data_Use_Agreement.pdf (accessed 11 August 2026).

Data Availability Statement: Data used in the preparation of this article were obtained from the Alzheimer's Disease Neuroimaging Initiative (ADNI) database (adni.loni.usc.edu, accessed 11 August 2026). The ADNI is a multicenter longitudinal study that collects clinical, neuropsychological, imaging, genetic, and biomarker data to investigate the progression of Alzheimer's disease across the cognitively unimpaired, mild cognitive impairment, and dementia stages. ADNI data are made available to approved researchers through the LONI Image and Data Archive. For additional information, see www.adni-info.org (accessed on 11 August 2026).

Acknowledgments: The data used in the preparation of this article were obtained from the ADNI database (adni.loni.usc.edu). As such, the investigators within the ADNI contributed to the design and implementation of the ADNI and/or provided data but did not participate in the analysis or writing of this report. A complete list of ADNI investigators can be found at https://adni.loni.usc.edu/wp-content/uploads/how_to_apply/ADNI_Acknowledgement_List.pdf (accessed on 11 August 2026).

Conflicts of Interest: The authors declare no conflicts of interest.

Abbreviations

The following abbreviations are used in this manuscript:

ADNI	Alzheimer's Disease Neuroimaging Initiative
CN	Cognitively normal
CSF	Cerebrospinal fluid
DTI	Diffusion tensor imaging
DTI-ALPS	Diffusion tensor image analysis along the perivascular space
dMRI	Diffusion magnetic resonance imaging
FA	Fractional anisotropy
MRI	Magnetic resonance imaging
ROI	Region of interest

References

1. Iliff, J.J.; Wang, M.; Liao, Y.; Plogg, B.A.; Peng, W.; Gundersen, G.A.; Benveniste, H.; Vates, G.E.; Deane, R.; Goldman, S.A.; et al. A paravascular pathway facilitates CSF flow through the brain parenchyma and the clearance of interstitial solutes, including amyloid β. *Sci. Transl. Med.* **2012**, *4*, 147ra111. [CrossRef] [PubMed]
2. Jessen, N.A.; Munk, A.S.F.; Lundgaard, I.; Nedergaard, M. The glymphatic system: A beginner's guide. *Neurochem. Res.* **2015**, *40*, 2583–2599. [CrossRef] [PubMed]
3. Benveniste, H.; Liu, X.; Koundal, S.; Sanggaard, S.; Lee, H.; Wardlaw, J. The glymphatic system and waste clearance with brain aging: A review. *Gerontology* **2019**, *65*, 106–119. [CrossRef] [PubMed]

4. Huang, S.Y.; Zhang, Y.R.; Guo, Y.; Du, J.; Ren, P.; Wu, B.S.; Feng, J.F.; Alzheimer's Disease Neuroimaging Initiative; Cheng, W.; Yu, J.T. Glymphatic system dysfunction predicts amyloid deposition, neurodegeneration, and clinical progression in Alzheimer's disease. *Alzheimer's Dement.* **2024**, *20*, 3251–3269. [CrossRef] [PubMed]
5. Lim, S.; Lee, Y.; Yun, C.S.; Kim, K.; Yun, C.H. Alzheimer's Disease Neuroimaging Initiative. Change in amyloid-β deposition and diffusion tensor image analysis along the perivascular space index in incident neurodegenerative disease. *Ann. Neurol.* **2026**, *100*, 559–571. [CrossRef] [PubMed]
6. Taoka, T.; Naganawa, S. Gadolinium-based contrast media, cerebrospinal fluid and the glymphatic system: Possible mechanisms for the deposition of gadolinium in the brain. *Magn. Reson. Med. Sci.* **2018**, *17*, 111–119. [CrossRef] [PubMed]
7. Ringstad, G.; Valnes, L.M.; Dale, A.M.; Pripp, A.H.; Vatnehol, S.S.; Emblem, K.E.; Mardal, K.A.; Eide, P.K. Brain-wide glymphatic Enhancement and clearance in humans assessed with MRI. *JCI Insight* **2018**, *3*, e121537. [CrossRef] [PubMed]
8. Zhang, M.; Tang, J.; Xia, D.; Xue, Y.; Ren, X.; Huang, Q.; Shi, L.; Tang, W.; Fu, J. Evaluation of glymphatic-meningeal lymphatic system with intravenous gadolinium-based contrast-enhancement in cerebral small-vessel disease. *Eur. Radiol.* **2023**, *33*, 6096–6106. [CrossRef] [PubMed]
9. Richmond, S.B.; Rane, S.; Hanson, M.R.; Albayram, M.; Iliff, J.J.; Kernagis, D.; Rosenberg, J.T.; Seidler, R.D. Quantification approaches for magnetic resonance imaging following intravenous gadolinium injection: A window into brain-wide glymphatic function. *Eur. J. Neurosci.* **2023**, *57*, 1689–1704. [CrossRef] [PubMed]
10. Calvo, N.; Jamil, M.; Feldman, S.; Shah, A.; Nauman, F.; Ferrara, J. Neurotoxicity from intrathecal gadolinium administration: Case presentation and brief review. *Neurol. Clin. Pract.* **2020**, *10*, e7–e10. [CrossRef] [PubMed]
11. Taoka, T.; Masutani, Y.; Kawai, H.; Nakane, T.; Matsuoka, K.; Yasuno, F.; Kishimoto, T.; Naganawa, S. Evaluation of glymphatic system activity with the diffusion MR technique: Diffusion tensor image analysis along the perivascular space (DTI-ALPS) in Alzheimer's disease cases. *Jpn. J. Radiol.* **2017**, *35*, 172–178. [CrossRef] [PubMed]
12. Örzsik, B.; Palombo, M.; Asllani, I.; Dijk, D.J.; Harrison, N.A.; Cercignani, M. Higher order diffusion imaging as a putative index of human sleep-related microstructural changes and glymphatic Clearance. *NeuroImage* **2023**, *274*, 120124. [CrossRef] [PubMed]
13. Demiral, Ş.B.; Tomasi, D.; Sarlls, J.; Lee, H.; Wiers, C.E.; Zehra, A.; Srivastava, T.; Ke, K.; Shokri-Kojori, E.; Freeman, C.R.; et al. Apparent diffusion coefficient changes in human brain during sleep—Does it inform on the existence of a glymphatic system? *NeuroImage* **2019**, *185*, 263–273. [CrossRef] [PubMed]
14. Gędek, A.; Koziorowski, D.; Szlufik, S. Assessment of factors influencing glymphatic activity and implications for clinical medicine. *Front. Neurol.* **2023**, *14*, 1232304. [CrossRef] [PubMed]
15. Chen, H.L.; Chen, P.C.; Lu, C.H.; Tsai, N.W.; Yu, C.C.; Chou, K.H.; Lai, Y.R.; Taoka, T.; Lin, W.C. Associations among cognitive functions, plasma DNA, and diffusion tensor image along the perivascular space (DTI-ALPS) in patients with Parkinson's disease. *Oxid. Med. Cell. Longev.* **2021**, *2021*, 4034509. [CrossRef] [PubMed]
16. Bao, W.; Jiang, P.; Xu, P.; Lin, H.; Xu, J.; Lai, M.; Yuan, J.; Xu, J. Lower DTI-ALPS index in patients with major depressive disorder: Correlation with fatigue. *Behav. Brain Res.* **2025**, *478*, 115323. [CrossRef] [PubMed]
17. Firbank, M.J.; Donaghy, P.C.; Allan, L.M.; Barnett, N.; Barker, S.H.; Ciafone, J.; Durcan, R.; Greenfinch, G.; Hamilton, C.A.; Olsen, K.; et al. Changes in DTI-ALPS index and its associations with neuronal damage in Lewy body disease. *Park. Relat. Disord.* **2025**, *140*, 108014. [CrossRef] [PubMed]
18. Costa, T.; Manuello, J.; Premi, E.; Mattioli, I.; Lasagna, L.; Lahoz, C.B.; Cauda, F.; Duca, S.; Liloia, D. Evaluating the robustness of DTI-ALPS in clinical context: A meta-analytic parallel on Alzheimer's and Parkinson's diseases. *Sci. Rep.* **2024**, *14*, 26381. [CrossRef] [PubMed]
19. Alvim, D.M.; Valdés Hernández, M.D.C.; Bastin, M.E.; Clancy, U.; Arteaga-Reyes, C.; Wiseman, S.; Jochems, A.C.C.; Garcia, D.J.; Hamilton, O.K.L.; Backhouse, E.V.; et al. Relevance of the diffusion tensor imaging along the perivascular space (DTI-ALPS) index in small vessel disease—A study in patients with mild ischaemic stroke. *Neurobiol. Aging* **2026**, *163*, 35–45. [CrossRef] [PubMed]
20. Vuong, N.; Lasič, S.; Hall, S.; Spotorno, N.; van Westen, D.V.; Hansson, O.; Nilsson, M.; Georgiopoulos, C. Balancing accuracy and precision: Optimal b-values for diffusion tensor imaging along the perivascular space. *AJNR Am. J. Neuroradiol.* **2026**, *47*, 1920–1926. [CrossRef] [PubMed]
21. Ajouz, A.; Jansen, O.; Frohwein, L.J.; Seehafer, S.; Larsen, N.; Hövener, J.B. Automatic determination of glymphatic flow with the DTI-ALPS-index along the principal axis system in native imaging space corrects for head and fiber orientation. *Magn. Reson. Med.* **2026**, *95*, 1110–1122. [CrossRef] [PubMed]
22. Tatekawa, H.; Matsushita, S.; Ueda, D.; Takita, H.; Horiuchi, D.; Atsukawa, N.; Morishita, Y.; Tsukamoto, T.; Shimono, T.; Miki, Y. Improved reproducibility of diffusion tensor image analysis along the perivascular space (DTI-ALPS) index: An analysis of reorientation technique of the OASIS-3 dataset. *Jpn. J. Radiol.* **2023**, *41*, 393–400. [CrossRef] [PubMed]
23. Taoka, T.; Ito, R.; Nakamichi, R.; Nakane, T.; Kawai, H.; Naganawa, S. Diffusion tensor image analysis along the perivascular space (DTI-ALPS): Revisiting the meaning and significance of the method. *Magn. Reson. Med. Sci.* **2024**, *23*, 268–290. [CrossRef] [PubMed]

24. Soares, J.M.; Marques, P.; Alves, V.; Sousa, N. A hitchhiker's guide to diffusion tensor imaging. *Front. Neurosci.* **2013**, *7*, 31. [CrossRef] [PubMed]
25. Tournier, J.D.; Smith, R.; Raffelt, D.; Tabbara, R.; Dhollander, T.; Pietsch, M.; Christiaens, D.; Jeurissen, B.; Yeh, C.H.; Connelly, A. MRtrix3: A fast, flexible and open software framework for medical image processing and visualisation. *NeuroImage* **2019**, *202*, 116137. [CrossRef] [PubMed]
26. Shapiro, S.S.; Wilk, M.B. An Analysis of Variance Test for Normality (Complete Samples). *Biometrika* **1965**, *52*, 591–611. [CrossRef]
27. Friedman, M. The Use of Ranks to Avoid the Assumption of Normality Implicit in the Analysis of Variance. *J. Am. Stat. Assoc.* **1937**, *32*, 675–701. [CrossRef]
28. Kellner, E.; Dhital, B.; Kiselev, V.G.; Reisert, M. Gibbs-ringing artifact removal based on local subvoxel-shifts. *Magn. Reson. Med.* **2016**, *76*, 1574–1581. [CrossRef] [PubMed]
29. Johnson, L.A.; Pearlman, J.D.; Miller, C.A.; Young, T.I.; Thulborn, K.R. MR Quantification of Cerebral Ventricular Volume Using a Semiautomated Algorithm. *AJNR Am. J. Neuroradiol.* **1993**, *14*, 1373–1378. [PubMed]
30. Veraart, J.; Fieremans, E.; Jelescu, I.O.; Knoll, F.; Novikov, D.S. Gibbs ringing in diffusion MRI. *Magn. Reson. Med.* **2016**, *76*, 301–314. [CrossRef] [PubMed]
31. Perrone, D.; Aelterman, J.; Pižurica, A.; Jeurissen, B.; Philips, W.; Leemans, A. The effect of Gibbs ringing artifacts on measures derived from diffusion MRI. *NeuroImage* **2015**, *120*, 441–455. [CrossRef] [PubMed]
32. Ling, J.; Merideth, F.; Caprihan, A.; Pena, A.; Teshiba, T.; Mayer, A.R. Head injury or head motion? Assessment and quantification of motion artifacts in diffusion tensor imaging studies. *Hum. Brain Mapp.* **2012**, *33*, 50–62. [CrossRef] [PubMed]
33. Jezzard, P.; Barnett, A.S.; Pierpaoli, C. Characterization of and correction for eddy current artifacts in echo planar diffusion imaging. *Magn. Reson. Med.* **1998**, *39*, 801–812. [CrossRef] [PubMed]
34. Kober, T.; Gruetter, R.; Krueger, G. Prospective and retrospective motion correction in diffusion magnetic resonance imaging of the human brain. *NeuroImage* **2012**, *59*, 389–398. [CrossRef] [PubMed]
35. Burles, F.; Sallis, E.; Kopala-Sibley, D.C.; Iaria, G. Alzheimer's Disease Neuroimaging Initiative. Mitigating head position bias in perivascular fluid imaging: LD-ALPS, a novel method for DTI-ALPS calculation. *NeuroSci* **2025**, *6*, 101. [CrossRef] [PubMed]
36. Sakaie, K.; Lowe, M. Retrospective correction of bias in diffusion tensor imaging arising from coil combination mode. *Magn. Reson. Imaging* **2017**, *37*, 203–208. [CrossRef] [PubMed]
37. Miloushev, V.Z.; Boltyanskiy, R.; Granlund, K.L.; Keshari, K.R. Improved total sensitivity estimation for multiple receive coils in MRI using ratios of first-order statistics. *Magn. Reson. Mater. Phys. Biol. Med.* **2022**, *35*, 895–901. [CrossRef] [PubMed]
38. Malyarenko, D.I.; Ross, B.D.; Chenevert, T.L. Analysis and correction of gradient nonlinearity bias in apparent diffusion coefficient measurements. *Magn. Reson. Med.* **2014**, *71*, 1312–1323. [CrossRef] [PubMed]
39. Mukherjee, P.; Chung, S.W.; Berman, J.I.; Hess, C.P.; Henry, R.G. Diffusion Tensor MR imaging and fiber tractography: Technical considerations. *AJNR Am. J. Neuroradiol.* **2008**, *29*, 843–852. [CrossRef] [PubMed]
40. Andersson, J.L.R. Maximum a posteriori estimation of diffusion tensor parameters using a Rician noise model: Why, how and but. *NeuroImage* **2008**, *42*, 1340–1356. [CrossRef] [PubMed]
41. Anderson, A.W. Theoretical analysis of the effects of noise on diffusion tensor imaging. *Magn. Reson. Med.* **2001**, *46*, 1174–1188. [CrossRef] [PubMed]
42. Batchelor, P.G.; Atkinson, D.; Hill, D.L.G.; Calamante, F.; Connelly, A. Anisotropic noise propagation in diffusion tensor MRI sampling schemes. *Magn. Reson. Med.* **2003**, *49*, 1143–1151. [CrossRef] [PubMed]
43. Liu, X.; Barisano, G.; Shao, X.; Jann, K.; Ringman, J.M.; Lu, H.; Arfanakis, K.; Caprihan, A.; DeCarli, C.; Gold, B.T.; et al. Cross-vendor test-retest validation of diffusion tensor image analysis along the perivascular space (DTI-ALPS) for evaluating glymphatic system function. *Aging Dis.* **2024**, *15*, 1885–1898. [CrossRef] [PubMed]

Disclaimer/Publisher's Note: The statements, opinions and data contained in all publications are solely those of the individual author(s) and contributor(s) and not of MDPI and/or the editor(s). MDPI and/or the editor(s) disclaim responsibility for any injury to people or property resulting from any ideas, methods, instructions or products referred to in the content.